Jet modification via π^0-hadron correlations in Au + Au collisions at $\sqrt{s_{NN}} = 200$ GeV

N. J. Abdulameer,[17,25] U. Acharya,[22] A. Adare,[13] S. Afanasiev,[33] C. Aidala,[47,49] N. N. Ajitanand,[71,*] Y. Akiba,[65,66,†] H. Al-Bataineh,[58] J. Alexander,[71] M. Alfred,[24] K. Aoki,[35,38,65] N. Apadula,[30,72] L. Aphecetche,[73] J. Asai,[65] H. Asano,[38,65] E. T. Atomssa,[39] R. Averbeck,[72] T. C. Awes,[61] B. Azmoun,[8] V. Babintsev,[26] M. Bai,[7] G. Baksay,[20] L. Baksay,[20] A. Baldisseri,[16] N. S. Bandara,[47] B. Bannier,[72] K. N. Barish,[9] P. D. Barnes,[42,*] B. Bassalleck,[57] A. T. Basye,[1] S. Bathe,[6,9,66] S. Batsouli,[61] V. Baublis,[64] C. Baumann,[8,51] A. Bazilevsky,[8] M. Beaumier,[9] S. Beckman,[13] S. Belikov,[8,*] R. Belmont,[13,59] R. Bennett,[72] A. Berdnikov,[68] Y. Berdnikov,[68] L. Bichon,[78] A. A. Bickley,[13] B. Blankenship,[78] D. S. Blau,[37,56] J. G. Boissevain,[42] J. S. Bok,[58] H. Borel,[16] V. Borisov,[68] K. Boyle,[66,72] M. L. Brooks,[42] J. Bryslawskyj,[6,9] H. Buesching,[8] V. Bumazhnov,[26] G. Bunce,[8,66] S. Butsyk,[42] C. M. Camacho,[42] S. Campbell,[14,30,72] B. S. Chang,[82] W. C. Chang,[2] J. L. Charvet,[16] C.-H. Chen,[66,72] D. Chen,[72] S. Chernichenko,[26] M. Chiu,[8,27] C. Y. Chi,[14] I. J. Choi,[27,82] J. B. Choi,[32,*] R. K. Choudhury,[5] T. Chujo,[76] P. Chung,[71] A. Churyn,[26] V. Cianciolo,[61] Z. Citron,[72,80] B. A. Cole,[14] M. Connors,[22,66] P. Constantin,[42] R. Corliss,[72] M. Csanád,[18] T. Csörgő,[48,81] D. d'Enterria,[39] T. Dahms,[72] S. Dairaku,[38,65] T. W. Danley,[60] K. Das,[21] A. Datta,[57] M. S. Daugherity,[1] G. David,[8,72] K. DeBlasio,[57] K. Dehmelt,[20,72] A. Denisov,[26] A. Deshpande,[66,72] E. J. Desmond,[8] O. Dietzsch,[69] A. Dion,[72] P. B. Diss,[46] M. Donadelli,[69] V. Doomra,[72] J. H. Do,[82] O. Drapier,[39] A. Drees,[72] K. A. Drees,[7] A. K. Dubey,[80] J. M. Durham,[42,72] A. Durum,[26] D. Dutta,[5] V. Dzhordzhadze,[9] Y. V. Efremenko,[61] F. Ellinghaus,[13] H. En'yo,[65,66] T. Engelmore,[14] A. Enokizono,[41,65,67] R. Esha,[72] K. O. Eyser,[8,9] B. Fadem,[52] N. Feege,[72] D. E. Fields,[57,66] M. Finger, Jr.,[10] M. Finger,[10] D. Firak,[17,72] D. Fitzgerald,[49] F. Fleuret,[39] S. L. Fokin,[37] Z. Fraenkel,[80,*] J. E. Frantz,[60,72] A. Franz,[8] A. D. Frawley,[21] K. Fujiwara,[65] Y. Fukao,[38,65] T. Fusayasu,[54] P. Gallus,[15] C. Gal,[72] P. Garg,[4,72] I. Garishvili,[41,74] H. Ge,[72] F. Giordano,[27] A. Glenn,[13,41] H. Gong,[72] M. Gonin,[39] J. Gosset,[16] Y. Goto,[65,66] R. Granier de Cassagnac,[39] N. Grau,[3,14] S. V. Greene,[78] M. Grosse Perdekamp,[27,66] T. Gunji,[12] T. Guo,[72] H.-Å. Gustafsson,[44,*] T. Hachiya,[23,65,66] A. Hadj Henni,[73] J. S. Haggerty,[8] K. I. Hahn,[19] H. Hamagaki,[12] H. F. Hamilton,[1] J. Hanks,[14,72] R. Han,[63] S. Y. Han,[19,36] E. P. Hartouni,[41] K. Haruna,[23] S. Hasegawa,[31] T. O. S. Haseler,[22] K. Hashimoto,[65,67] E. Haslum,[44] R. Hayano,[12] M. Heffner,[41] T. K. Hemmick,[72] T. Hester,[9] X. He,[22] J. C. Hill,[30] A. Hodges,[22,27] M. Hohlmann,[20] R. S. Hollis,[9] W. Holzmann,[71] K. Homma,[23] B. Hong,[36] T. Horaguchi,[12,65,75] D. Hornback,[74] T. Hoshino,[23] N. Hotvedt,[30] J. Huang,[8] T. Ichihara,[65,66] R. Ichimiya,[65] H. Iinuma,[38,65] Y. Ikeda,[76] K. Imai,[31,38,65] J. Imrek,[17] M. Inaba,[76] A. Iordanova,[9] D. Isenhower,[1] M. Ishihara,[65] T. Isobe,[12,65] M. Issah,[71] A. Isupov,[33] D. Ivanishchev,[64] B. V. Jacak,[72] M. Jezghani,[22] X. Jiang,[42] J. Jin,[14] Z. Ji,[72] B. M. Johnson,[8,22] K. S. Joo,[53] D. Jouan,[62] D. S. Jumper,[1,27] F. Kajihara,[12] S. Kametani,[65] N. Kamihara,[66] J. Kamin,[72] S. Kanda,[12] J. H. Kang,[82] J. Kapustinsky,[42] D. Kawall,[47,66] A. V. Kazantsev,[37] T. Kempel,[30] J. A. Key,[57] V. Khachatryan,[72] A. Khanzadeev,[64] K. M. Kijima,[23] J. Kikuchi,[79] B. Kimelman,[52] B. I. Kim,[36] C. Kim,[36] D. H. Kim,[53] D. J. Kim,[34,82] E. Kim,[70] E.-J. Kim,[32] G. W. Kim,[19] M. Kim,[70] S. H. Kim,[82] E. Kinney,[13] K. Kiriluk,[13] Á. Kiss,[18] E. Kistenev,[8] R. Kitamura,[12] J. Klatsky,[21] J. Klay,[41] C. Klein-Boesing,[51] D. Kleinjan,[9] P. Kline,[72] T. Koblesky,[13] L. Kochenda,[64] B. Komkov,[64] M. Konno,[76] J. Koster,[27] D. Kotov,[64,68] L. Kovacs,[18] A. Kozlov,[80] A. Kravitz,[14] A. Král,[15] G. J. Kunde,[42] B. Kurgyis,[18,72] K. Kurita,[65,67] M. Kurosawa,[65,66] M. J. Kweon,[36] Y. Kwon,[74,82] G. S. Kyle,[58] Y. S. Lai,[14] J. G. Lajoie,[30] D. Layton,[27] A. Lebedev,[30] D. M. Lee,[42] K. B. Lee,[36] S. Lee,[82] S. H. Lee,[30,72] T. Lee,[70] M. J. Leitch,[42] M. A. L. Leite,[69] B. Lenzi,[69] P. Liebing,[66] S. H. Lim,[82] A. Litvinenko,[33] H. Liu,[58] M. X. Liu,[42] T. Liška,[15] X. Li,[11] S. Lokos,[81] D. A. Loomis,[49] B. Love,[78] D. Lynch,[8] C. F. Maguire,[78] Y. I. Makdisi,[7] M. Makek,[83] A. Malakhov,[33] M. D. Malik,[57] A. Manion,[72] V. I. Manko,[37] E. Mannel,[8,14] Y. Mao,[63,65] H. Masui,[76] F. Matathias,[14] L. Mašek,[10,29] M. McCumber,[42,72] P. L. McGaughey,[42] D. McGlinchey,[13,42] C. McKinney,[27] N. Means,[72] A. Meles,[58] M. Mendoza,[9] B. Meredith,[27] Y. Miake,[76] A. C. Mignerey,[46] P. Mikeš,[29] K. Miki,[76] A. Milov,[8,80] D. K. Mishra,[5] M. Mishra,[4] J. T. Mitchell,[8] M. Mitrankova,[68,72] Iu. Mitrankov,[68,72] S. Miyasaka,[65,75] S. Mizuno,[65,76] A. K. Mohanty,[5] P. Montuenga,[27] T. Moon,[36,82] Y. Morino,[12] A. Morreale,[9] D. P. Morrison,[8] T. V. Moukhanova,[37] D. Mukhopadhyay,[78] B. Mulilo,[36,65,84] T. Murakami,[38,65] J. Murata,[65,67] A. Mwai,[71] S. Nagamiya,[35,65] K. Nagashima,[23] J. L. Nagle,[13] M. Naglis,[80] M. I. Nagy,[18] I. Nakagawa,[65,66] H. Nakagomi,[65,76] Y. Nakamiya,[23] T. Nakamura,[23] K. Nakano,[65,75] C. Nattrass,[74] P. K. Netrakanti,[5] J. Newby,[41] M. Nguyen,[72] T. Niida,[76] S. Nishimura,[12] R. Nouicer,[8,66] N. Novitzky,[34,72] T. Novák,[48,81] G. Nukazuka,[65,66] A. S. Nyanin,[37] E. O'Brien,[8] S. X. Oda,[12] C. A. Ogilvie,[30] K. Okada,[66] M. Oka,[76] Y. Onuki,[65] J. D. Orjuela Koop,[13] M. Orosz,[17,25] J. D. Osborn,[49,61] A. Oskarsson,[44] M. Ouchida,[23] K. Ozawa,[12,35,76] R. Pak,[8] A. P. T. Palounek,[42] V. Pantuev,[28,72] V. Papavassiliou,[58] J. Park,[70] J. S. Park,[70] S. Park,[50,65,70,72] W. J. Park,[36] M. Patel,[30] S. F. Pate,[58] H. Pei,[30] J.-C. Peng,[27] H. Pereira,[16] D. V. Perepelitsa,[8,13] G. D. N. Perera,[58] V. Peresedov,[33] D.Yu. Peressounko,[37] J. Perry,[30] R. Petti,[8,72] C. Pinkenburg,[8] R. Pinson,[1] R. P. Pisani,[8] M. Potekhin,[8] M. L. Purschke,[8] A. K. Purwar,[42] H. Qu,[22] A. Rakotozafindrabe,[39] J. Rak,[34,57] B. J. Ramson,[49] I. Ravinovich,[80] K. F. Read,[61,74] S. Rembeczki,[20] K. Reygers,[51] D. Reynolds,[71] V. Riabov,[56,64] Y. Riabov,[64,68] D. Richford,[6,77] T. Rinn,[30] D. Roach,[78] G. Roche,[43,*] S. D. Rolnick,[9] M. Rosati,[30] S. S. E. Rosendahl,[44] P. Rosnet,[43] Z. Rowan,[6] J. G. Rubin,[49] P. Rukoyatkin,[33] P. Ružička,[29]

[*] Deceased.

[†] Contact author: akiba@rcf.rhic.bnl.gov

V. L. Rykov,[65] B. Sahlmueller,[51,72] N. Saito,[35,38,65,66] T. Sakaguchi,[8] S. Sakai,[76] K. Sakashita,[65,75] H. Sako,[31] V. Samsonov,[56,64] M. Sarsour,[22] S. Sato,[31,35] T. Sato,[76] S. Sawada,[35] B. Schaefer,[78] B. K. Schmoll,[74] K. Sedgwick,[9] J. Seele,[13] R. Seidl,[27,65,66] A.Yu. Semenov,[30] V. Semenov,[26,28] A. Sen,[30,74] R. Seto,[9] P. Sett,[5] A. Sexton,[46] D. Sharma,[72,80] I. Shein,[26] Z. Shi,[42] T.-A. Shibata,[65,75] K. Shigaki,[23] M. Shimomura,[30,55,76] K. Shoji,[38,65] P. Shukla,[5] A. Sickles,[8,27] C. L. Silva,[42,69] D. Silvermyr,[44,61] C. Silvestre,[16] K. S. Sim,[36] B. K. Singh,[4] C. P. Singh,[4,*] V. Singh,[4] M. Slunečka,[10] K. L. Smith,[21,42] M. Snowball,[42] A. Soldatov,[26] R. A. Soltz,[41] W. E. Sondheim,[42] S. P. Sorensen,[74] I. V. Sourikova,[8] F. Staley,[16] P. W. Stankus,[61] E. Stenlund,[44] M. Stepanov,[47,58,*] A. Ster,[81] S. P. Stoll,[8] T. Sugitate,[23] C. Suire,[62] A. Sukhanov,[8] T. Sumita,[65] J. Sun,[72] Z. Sun,[17,25,72] J. Sziklai,[81] E. M. Takagui,[69] A. Taketani,[65,66] R. Tanabe,[76] Y. Tanaka,[54] K. Tanida,[31,65,66,70] M. J. Tannenbaum,[8] S. Tarafdar,[78,80] A. Taranenko,[56,71] P. Tarján,[17] H. Themann,[72] T. L. Thomas,[57] R. Tieulent,[22,45] A. Timilsina,[30] T. Todoroki,[65,66,76] M. Togawa,[38,65] A. Toia,[72] Y. Tomita,[76] L. Tomášek,[29] M. Tomášek,[15,29] H. Torii,[23,65] C. L. Towell,[1] R. Towell,[1] R. S. Towell,[1] V-N. Tram,[39] I. Tserruya,[80] Y. Tsuchimoto,[23] B. Ujvari,[17,25] C. Vale,[30] H. Valle,[78] H. W. van Hecke,[42] A. Veicht,[14,27] J. Velkovska,[78] A. A. Vinogradov,[37] M. Virius,[15] V. Vrba,[15,29] E. Vznuzdaev,[64] R. Vértesi,[17,81] X. R. Wang,[58,66] Y. Watanabe,[65,66] Y. S. Watanabe,[12,35] F. Wei,[30,58] J. Wessels,[51] A. S. White,[49] S. N. White,[8] D. Winter,[14] C. P. Wong,[8,22,42] C. L. Woody,[8] M. Wysocki,[13,61] B. Xia,[60] W. Xie,[66] L. Xue,[22] S. Yalcin,[72] Y. L. Yamaguchi,[12,72,79] K. Yamaura,[23] R. Yang,[27] A. Yanovich,[26] J. Ying,[22] S. Yokkaichi,[65,66] I. Yoon,[70] J. H. Yoo,[36] G. R. Young,[61] I. Younus,[40,57] I. E. Yushmanov,[37] H. Yu,[58,63] W. A. Zajc,[14] O. Zaudtke,[51] A. Zelenski,[7] C. Zhang,[61] S. Zhou,[11] L. Zolin,[33] and L. Zou[9]

(PHENIX Collaboration)

[1]*Abilene Christian University, Abilene, Texas 79699, USA*

[2]*Institute of Physics, Academia Sinica, Taipei 11529, Taiwan*

[3]*Department of Physics, Augustana University, Sioux Falls, South Dakota 57197, USA*

[4]*Department of Physics, Banaras Hindu University, Varanasi 221005, India*

[5]*Bhabha Atomic Research Centre, Bombay 400 085, India*

[6]*Baruch College, City University of New York, New York, New York 10010 USA*

[7]*Collider-Accelerator Department, Brookhaven National Laboratory, Upton, New York 11973-5000, USA*

[8]*Physics Department, Brookhaven National Laboratory, Upton, New York 11973-5000, USA*

[9]*University of California-Riverside, Riverside, California 92521, USA*

[10]*Charles University, Faculty of Mathematics and Physics, 180 00 Troja, Prague, Czech Republic*

[11]*Science and Technology on Nuclear Data Laboratory, China Institute of Atomic Energy, Beijing 102413, People's Republic of China*

[12]*Center for Nuclear Study, Graduate School of Science, University of Tokyo, 7-3-1 Hongo, Bunkyo, Tokyo 113-0033, Japan*

[13]*University of Colorado, Boulder, Colorado 80309, USA*

[14]*Columbia University, New York, New York 10027 and Nevis Laboratories, Irvington, New York 10533, USA*

[15]*Czech Technical University, Zikova 4, 166 36 Prague 6, Czech Republic*

[16]*Dapnia, CEA Saclay, F-91191, Gif-sur-Yvette, France*

[17]*Debrecen University, H-4010 Debrecen, Egyetem tér 1, Hungary*

[18]*ELTE, Eötvös Loránd University, H-1117 Budapest, Pázmány P. s. 1/A, Hungary*

[19]*Ewha Womans University, Seoul 120-750, Korea*

[20]*Florida Institute of Technology, Melbourne, Florida 32901, USA*

[21]*Florida State University, Tallahassee, Florida 32306, USA*

[22]*Georgia State University, Atlanta, Georgia 30303, USA*

[23]*Physics Program and International Institute for Sustainability with Knotted Chiral Meta Matter (SKCM2), Hiroshima University, Higashi-Hiroshima, Hiroshima 739-8526, Japan*

[24]*Department of Physics and Astronomy, Howard University, Washington, DC 20059, USA*

[25]*HUN-REN ATOMKI, H-4026 Debrecen, Bem tér 18/c, Hungary*

[26]*IHEP Protvino, State Research Center of Russian Federation, Institute for High Energy Physics, Protvino 142281, Russia*

[27]*University of Illinois at Urbana-Champaign, Urbana, Illinois 61801, USA*

[28]*Institute for Nuclear Research of the Russian Academy of Sciences, prospekt 60-letiya Oktyabrya 7a, Moscow 117312, Russia*

[29]*Institute of Physics, Academy of Sciences of the Czech Republic, Na Slovance 2, 182 21 Prague 8, Czech Republic*

[30]*Iowa State University, Ames, Iowa 50011, USA*

[31]*Advanced Science Research Center, Japan Atomic Energy Agency, 2-4 Shirakata Shirane, Tokai-mura, Naka-gun, Ibaraki-ken 319-1195, Japan*

[32]*Jeonbuk National University, Jeonju, 54896, Korea*

[33]*Joint Institute for Nuclear Research, 141980 Dubna, Moscow Region, Russia*

[34]*Helsinki Institute of Physics and University of Jyväskylä, P.O.Box 35, FI-40014 Jyväskylä, Finland*

[35]*KEK, High Energy Accelerator Research Organization, Tsukuba, Ibaraki 305-0801, Japan*

[36]*Korea University, Seoul 02841, Korea*

[37]*National Research Center "Kurchatov Institute", Moscow 123098, Russia*

[38]*Kyoto University, Kyoto 606-8502, Japan*

[39]*Laboratoire Leprince-Ringuet, Ecole Polytechnique, CNRS-IN2P3, Route de Saclay, F-91128 Palaiseau, France*

[40]*Physics Department, Lahore University of Management Sciences, Lahore 54792, Pakistan*
[41]*Lawrence Livermore National Laboratory, Livermore, California 94550, USA*
[42]*Los Alamos National Laboratory, Los Alamos, New Mexico 87545, USA*
[43]*LPC, Université Blaise Pascal, CNRS-IN2P3, Clermont-Fd, 63177 Aubiere Cedex, France*
[44]*Department of Physics, Lund University, Box 118, SE-221 00 Lund, Sweden*
[45]*IPNL, CNRS/IN2P3, Univ Lyon, Université Lyon 1, F-69622 Villeurbanne, France*
[46]*University of Maryland, College Park, Maryland 20742, USA*
[47]*Department of Physics, University of Massachusetts, Amherst, Massachusetts 01003-9337, USA*
[48]*MATE, Laboratory of Femtoscopy, Károly Róbert Campus, H-3200 Gyöngyös, Mátraiút 36, Hungary*
[49]*Department of Physics, University of Michigan, Ann Arbor, Michigan 48109-1040, USA*
[50]*Mississippi State University, Mississippi State, Mississippi 39762, USA*
[51]*Institut für Kernphysik, University of Münster, D-48149 Münster, Germany*
[52]*Muhlenberg College, Allentown, Pennsylvania 18104-5586, USA*
[53]*Myongji University, Yongin, Kyonggido 449-728, Korea*
[54]*Nagasaki Institute of Applied Science, Nagasaki-shi, Nagasaki 851-0193, Japan*
[55]*Nara Women's University, Kita-uoya Nishi-machi Nara 630-8506, Japan*
[56]*National Research Nuclear University, MEPhI, Moscow Engineering Physics Institute, Moscow 115409, Russia*
[57]*University of New Mexico, Albuquerque, New Mexico 87131, USA*
[58]*New Mexico State University, Las Cruces, New Mexico 88003, USA*
[59]*Physics and Astronomy Department, University of North Carolina at Greensboro, Greensboro, North Carolina 27412, USA*
[60]*Department of Physics and Astronomy, Ohio University, Athens, Ohio 45701, USA*
[61]*Oak Ridge National Laboratory, Oak Ridge, Tennessee 37831, USA*
[62]*IPN-Orsay, Université Paris-Sud, CNRS/IN2P3, Université Paris-Saclay, BP1, F-91406 Orsay, France*
[63]*Peking University, Beijing 100871, People's Republic of China*
[64]*PNPI, Petersburg Nuclear Physics Institute, Gatchina, Leningrad region 188300, Russia*
[65]*RIKEN Nishina Center for Accelerator-Based Science, Wako, Saitama 351-0198, Japan*
[66]*RIKEN BNL Research Center, Brookhaven National Laboratory, Upton, New York 11973-5000, USA*
[67]*Physics Department, Rikkyo University, 3-34-1 Nishi-Ikebukuro, Toshima, Tokyo 171-8501, Japan*
[68]*Saint Petersburg State Polytechnic University, St. Petersburg 195251, Russia*
[69]*Universidade de São Paulo, Instituto de Física, Caixa Postal 66318, São Paulo CEP05315-970, Brazil*
[70]*Department of Physics and Astronomy, Seoul National University, Seoul 151-742, Korea*
[71]*Chemistry Department, Stony Brook University, SUNY, Stony Brook, New York 11794-3400, USA*
[72]*Department of Physics and Astronomy, Stony Brook University, SUNY, Stony Brook, New York 11794-3800, USA*
[73]*SUBATECH (Ecole des Mines de Nantes, CNRS-IN2P3, Université de Nantes) BP 20722-44307, Nantes, France*
[74]*University of Tennessee, Knoxville, Tennessee 37996, USA*
[75]*Department of Physics, Tokyo Institute of Technology, Oh-okayama, Meguro, Tokyo 152-8551, Japan*
[76]*Tomonaga Center for the History of the Universe, University of Tsukuba, Tsukuba, Ibaraki 305, Japan*
[77]*United States Merchant Marine Academy, Kings Point, New York 11024, USA*
[78]*Vanderbilt University, Nashville, Tennessee 37235, USA*
[79]*Waseda University, Advanced Research Institute for Science and Engineering, 17 Kikui-cho, Shinjuku-ku, Tokyo 162-0044, Japan*
[80]*Weizmann Institute, Rehovot 76100, Israel*
[81]*Institute for Particle and Nuclear Physics, HUN-REN Wigner Research Centre for Physics (HUN-REN Wigner RCP, RMI), H-1525 Budapest 114, POBox 49, Budapest, Hungary*
[82]*Yonsei University, IPAP, Seoul 120-749, Korea*
[83]*Department of Physics, Faculty of Science, University of Zagreb, Bijenička c. 32 HR-10002 Zagreb, Croatia*
[84]*Department of Physics, School of Natural Sciences, University of Zambia, Great East Road Campus, Box 32379, Lusaka, Zambia*

(Received 13 June 2024; accepted 9 September 2024; published 1 October 2024)

High-momentum two-particle correlations are a useful tool for studying jet-quenching effects in the quark-gluon plasma. Angular correlations between neutral-pion triggers and charged hadrons with transverse momenta in the range 4–12 GeV/c and 0.5–7 GeV/c, respectively, have been measured by the PHENIX experiment in 2014 for Au + Au collisions at $\sqrt{s_{NN}} = 200$ GeV. Suppression is observed in the yield of high-momentum jet fragments opposite the trigger particle, which indicates jet suppression stemming from in-medium partonic energy loss, while enhancement is observed for low-momentum particles. The ratio and differences between the yield in Au + Au collisions and $p + p$ collisions, I_{AA} and Δ_{AA}, as a function of the trigger-hadron azimuthal separation, $\Delta\phi$, are measured for the first time at the BNL Relativistic Heavy Ion Collider. These results better

quantify how the yield of low-p_T associated hadrons is enhanced at wide angle, which is crucial for studying energy loss as well as medium-response effects.

DOI: 10.1103/PhysRevC.110.044901

I. INTRODUCTION

Jets, collimated sprays of energetic particles originating from the fragmentation of hard-scattered partons, are an important probe of the quark-gluon plasma (QGP) created in ultra-relativistic collisions of heavy ions, such as those at the BNL Relativistic Heavy Ion Collider (RHIC) and the CERN Large Hadron Collider (LHC) [1]. In particular, these hard-scattered partons interact with the QGP and lose energy when traveling through the medium before fragmenting into final-state jet particles. This partonic energy loss gives rise to jets that have been modified relative to jets that are measured in $p+p$ collisions, where no QGP medium is formed. The momentum distribution as well as the spatial distribution of particles within the resulting jets in particular are seen to be modified [2–6]. Measurements of jet modification allow for direct quantification of the energy transport properties of the medium [7]. Once the parton shower interacts with the QGP, the jets and medium particles are intrinsically coupled to one another. Therefore, the observed modifications can also embody a response from the QGP, which is often referred to as a medium response [8,9].

High-transverse-momentum neutral pions, π^0, can be reconstructed via their two-photon decay channel and used as jet proxies as they carry a large fraction of the jet momentum. Measuring the angular correlations between the π^0 and charged hadrons in the event, reveals how charged hadrons are distributed in the jet triggered by the π^0 as well as the opposing jet that appears 180 degrees away from the π^0. This phenomenon is depicted in Fig. 1. The angle, $\Delta\phi$, measures the azimuthal separation between the trigger π^0 and each associated particle. The jet containing the trigger π^0 labeled "near side" shows the trigger π^0 itself at $\Delta\phi = 0$, surrounded by "near side" associated particles. The recoil jet labeled "away side" shows the associated particles with $\Delta\phi \approx \pi$. The abundance of neutral pions, which can be reconstructed using the high-granularity PHENIX electromagnetic calorimeter (EMCal) out to high p_T, are great candidates for trigger particles. Two-particle correlations, such as π^0-hadron correlations, are preferred over full-jet reconstruction for dijet measurements in PHENIX to overcome the limited PHENIX acceptance.

The previous π^0-hadron correlations results from PHENIX [10] used an earlier and smaller data set from 2007. In subtraction of the underlying event, the third- and fourth-order harmonics, v_3 and v_4, were not considered. Therefore, the correlations related to jets were not fully decoupled from correlations with the underlying event. The 2014 results presented here use the largest Au + Au data set ever collected by PHENIX and include underlying event subtraction using updated measurements of the higher-order harmonic terms. The improved statistical precision and purity of the measurement enables comparisons of the away-side correlation yield in Au + Au to that in $p+p$ as a function of $\Delta\phi$, which provides insight into how the distribution of particles correlated with the jet is modified.

II. EXPERIMENT

Figure 2 shows the 2014 detector configuration. In this study, the PHENIX collaboration processed 5×10^9 minimum-bias events triggered by the PHENIX beam-beam counters [11] and collected by the central-arm detectors [12] for Au + Au collisions at $\sqrt{s_{NN}} = 200$ GeV. The $p+p$ collision data at $\sqrt{s_{NN}} = 200$ GeV were collected by PHENIX in 2006 and used 3.2×10^6 high-p_T photon-triggered events for baseline measurements [10].

III. DATA ANALYSIS

The π^0's, which are used as a jet proxy in this analysis, are reconstructed from their decay photons by pairing together EMCal clusters with an energy of 1 GeV or greater. To remove contamination from charged particles, EMCal clusters are required to be greater than 8 cm away from the closest track projection from the drift chambers to the EMCal. Additionally, a cut is made on the cluster shape to remove further potential contamination from hadrons. The photon pairs must have an energy asymmetry ($\alpha = \frac{|E_{\gamma_1} - E_{\gamma_2}|}{E_{\gamma_1} + E_{\gamma_2}}$, where E_{γ_1} and E_{γ_2} are the energies of the first and second photon, respectively) of less than 80% of the sum of the photon energy. Finally, each reconstructed π^0 is required to have an invariant mass between 0.12 and 0.16 GeV/c^2. Reconstructed π^0's used as jet proxies in this analysis have transverse momenta, p_{T,π^0}, of 4–12 GeV/c.

Reconstructed π^0's are then paired with reconstructed charged tracks. Reconstructed tracks are required to have $0.5 \leqslant p_{T,h} \leqslant 7$ GeV/c, where the upper limit of 7 GeV/c is chosen to limit contamination from secondaries produced by high-p_T hadrons within the detector that are mis-reconstructed as high-p_T tracks.

The $\Delta\phi$ correlation functions between π^0's and associated charged hadrons are normalized by the number of π^0's, N_{π^0} and then corrected for the single-hadron reconstruction

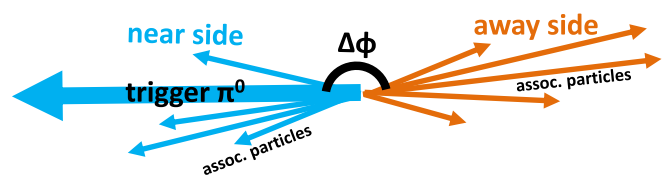

FIG. 1. Cartoon of two back-to-back jets as a spray of particles. The indicated angle, $\Delta\phi$, measures the azimuthal separation between the trigger π^0 and each associated particle. The jet labeled "near side" contains the trigger π^0 at $\Delta\phi = 0$. The jet labeled "away side" shows the constituents of the recoil jet at $\Delta\phi \approx \pi$.

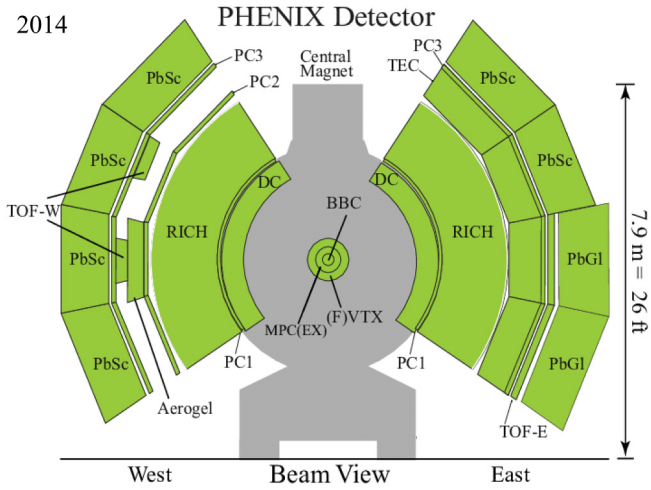

FIG. 2. Configuration of PHENIX central arm detector in 2014.

efficiency, ϵ, and the detector acceptance via simulation and event mixing. To obtain the correlation functions purely from jets, correlations due to the underlying event and flow are subtracted from the correlation functions. Then, the jet function, which is the differential yield of jet-associated π^0-hadron pairs per number of π^0's in a given π^0 p_T bin, N_{π^0-h}, with respect to $\Delta\phi$, can be written as

$$\frac{1}{N_{\pi^0}}\frac{dN_{\pi^0-h}}{d\Delta\phi} = \frac{1}{N_{\pi^0}}\frac{N_{\pi^0-h}}{\epsilon\int d\Delta\phi}\left\{\frac{dN^{\text{same}}_{\pi^0-h}/d\Delta\phi}{dN^{\text{mix}}_{\pi^0-h}/d\Delta\phi} - b_0\left[1+2\sum_{n=2}^{4}\langle v_n^{\pi^0}v_n^h\rangle\cos(n\cdot\Delta\phi)\right]\right\}, \quad (1)$$

where $N^{\text{same}}_{\pi^0-h}$ and $N^{\text{mix}}_{\pi^0-h}$ are the number of same-event and mixed-event π^0-hadron pairs, respectively.

The contribution to the correlation due to flow appears in the second term of Eq. (1) as a Fourier series in terms of the azimuthal correlation angle. The coefficient b_0 of the Fourier series is the magnitude of the underlying event estimated using zero-yield-at-minimum method (ZYAM) and absolute background normalization method (ABS) [13] in low $p_{T,h} < 1$ GeV/c and high $p_{T,h} \geqslant 1$ GeV/c, respectively. To improve the purity of the extracted jet-hadron correlation signal, the second to the fourth-order harmonics are subtracted ($v_2 - v_4$). The first-order harmonic (v_1) is not accounted for because its contribution is expected to be negligible at midrapidity [14,15]. The nth-order flow-harmonic coefficients are factorized to $v_n^{\pi^0}$ and v_n^h for π^0's and charged hadrons, respectively.

The π^0 $v_2^{\pi^0}$ and charged hadron v_n^h in Au + Au collisions at 200 GeV come from previous PHENIX measurements [16,17]. However, the higher-order π^0 flow-harmonic coefficients $n = 3, 4$ in these momentum ranges have not been measured at RHIC energies. Thus, to estimate $v_3^{\pi^0}$ and $v_4^{\pi^0}$, acoustic scaling [18] is applied. Acoustic scaling is the observation that there is a p_T-independent relation between different powers of the various flow harmonics given by the scaling factors, g_n, defined as

$$g_n = \frac{v_n}{(v_2)^{n/2}}. \quad (2)$$

Assuming the scaling factors of π^0's and charged hadron are approximately equal due to isospin symmetry (i.e., $g_n^h = g_n^{\pi^0}$), $v_3^{\pi^0}$ and $v_4^{\pi^0}$ can then be approximated by rearranging Eq. (2) to become

$$v_n^{\pi^0} = g_n^h \cdot \left(v_2^{\pi^0}\right)^{n/2}. \quad (3)$$

Modification to the per-jet integrated yield of hadrons is quantified by the yield-modification factor I_{AA}, defined as

$$I_{AA}(p_{T,h}) = \frac{\int_{\pi/2}^{3\pi/2}\left[dN^{\text{AuAu}}_{\pi^0-h}/d\Delta\phi\right]\cdot d\Delta\phi}{\int_{\pi/2}^{3\pi/2}\left[dN^{pp}_{\pi^0-h}/d\Delta\phi\right]\cdot d\Delta\phi}. \quad (4)$$

The I_{AA} is defined as the ratio of the integrated per-trigger yield of the away-side jet function within $\frac{\pi}{2} \leqslant \Delta\phi \leqslant \frac{3\pi}{2}$ in Au + Au to that measured in $p + p$ collisions. Additionally, for the first time at RHIC, the I_{AA} as a function of $\Delta\phi$, has been measured and is defined as the point-by-point ratio of per-trigger yield of the away-side jet function in Au + Au and $p + p$, that is,

$$I_{AA}(\Delta\phi) = \frac{dN^{\text{AuAu}}_{\pi^0-h}/d\Delta\phi}{dN^{pp}_{\pi^0-h}/d\Delta\phi}. \quad (5)$$

Downward fluctuations can cause negative yield at a particular $\Delta\phi$ bin. In such cases, the I_{AA} point is not shown. Additionally, for clarity, data points with a relative statistical or systematic uncertainty equal to or greater than 100% are also not shown.

Because $I_{AA}(\Delta\phi)$ in regions with small yield in Au + Au can be inflated through dividing by yields in $p + p$ close to zero, a complimentary observable that can also be extracted is the difference between the yields in Au + Au and $p + p$, that is,

$$\Delta_{AA}(\Delta\phi) = \frac{dN^{\text{AuAu}}_{\pi^0-h}}{d\Delta\phi} - \frac{dN^{pp}_{\pi^0-h}}{d\Delta\phi}. \quad (6)$$

IV. SYSTEMATIC UNCERTAINTY

Seven sources of systematic uncertainty are considered in this analysis. The first three arise from the second- to fourth-order flow-harmonic coefficients. The fourth is the estimation of the underlying event magnitude, b_0, using either ZYAM or ABS. The fifth arises from π^0 reconstruction. The sixth source is the single particle efficiency, which is represented by a global scale uncertainty of 6.9%. The seventh and final source of systematic uncertainty comes from the $p + p$ measurement used in this analysis, which is discussed in detail in Ref. [10].

The uncertainties from flow-harmonic coefficients are estimated by setting the coefficients to their upper and lower limits individually (including the uncertainty of the corresponding scaling factor), re-extracting the jet functions, and then recalculating the observable of interest. The relative uncertainties from the flow-harmonic coefficients are within a few percent at $p_{T,h} > 1$ GeV/c. Note that, the even-order-flow-harmonic coefficients do not contribute to the integrated-yield-modification measurements because the

integral of the even cosine terms equals zero. However, in the lowest $p_{T,h}$ bin where ZYAM is used in the flow subtraction, b_0 is allowed to vary in the uncertainties analyses due to flow-harmonic coefficients causing larger uncertainty ranges between 10%–30% in both differential and integrated yield-modification measurements.

The uncertainties arising from b_0 itself are estimated by varying the b_0 obtained from ZYAM and ABS to its upper and lower limits. These relative uncertainties are dominant at $p_{T,h} < 3$ GeV/c. The relative uncertainties from ABS ranges within 10% at $p_{T,h} > 1$ GeV/c, while the relative uncertainty from ZYAM ranges between 10%–50% at the lowest $p_{T,h}$ bin.

The uncertainty from π^0 reconstruction is estimated for each $p_{T,\pi^0} \otimes p_{T,h}$ bin via side-band analysis which involves remeasuring the jet functions using photon pairs with an invariant mass within 0.65–0.11 GeV/c^2 or 0.165–0.2 GeV/c^2, instead of the nominal π^0 mass window, 0.12–0.16 GeV/c^2. The π^0 reconstruction contribution becomes one of the dominant sources of uncertainty as $p_{T,h}$ increases. The relative uncertainty from π^0 reconstruction rises from a few percent to 20%.

Another dominant source of uncertainty at high $p_{T,h}$ comes from the $p + p$ collision data. The relative uncertainty from that increases from a few percent at $2 < p_{T,h} < 3$ GeV/c to 20% at $5 < p_{T,h} < 7$ GeV/c.

Except the global scaled uncertainty from single particle efficiency, uncertainties from other sources are correlated data-point-to-data-point. Note that, because the uncertainty from π^0 reconstruction is estimated as a function of p_T, it is a correlated uncertainty for $I_{AA}(p_T)$, but a global scaled uncertainty for $I_{AA}(\Delta\phi)$ and $\Delta_{AA}(\Delta\phi)$.

V. RESULTS

Figure 3 shows the jet functions after subtracting the underlying event from the correlation functions in the $5 < p_{T,\pi^0} < 7 \otimes 0.5 < p_{T,h} < 1$ GeV/c and $5 < p_{T,\pi^0} < 7 \otimes 2 < p_{T,h} < 4$ GeV/c momentum bins going left to right, and in the 0%–20% and 20%–40% going from top to bottom. The away-side jet peaks shown in Fig. 3 appear closer to a Gaussian function compared to previous PHENIX results [10], where there were pronounced peaks appearing to the left and right of the away-side jet peak, a phenomenon often attributed to a "mach-cone" effect created by supersonic traversal of the QGP by hard-scattered partons. However, such an effect is no longer seen once contamination from the third and fourth harmonics is removed. These changes are more pronounced at low $p_{T,h}$ where the underlying event is large.

The away-side I_{AA} as a function of the associated-hadron momentum, $I_{AA}(p_{T,h})$, is shown in Fig. 4 for four π^0 momentum ranges and in two centrality classes.

In each π^0 momentum range, the $I_{AA}(p_{T,h})$ is above unity at low $p_{T,h}$, but falls as $p_{T,h}$ increases, eventually reaching below unity at high $p_{T,h}$. The behavior of the I_{AA} at low-associated hadron momentum indicates that there is an enhancement in the yield of soft particles in central Au + Au collisions, whereas the subunity of the I_{AA} at high p_T is consistent with a suppression in the yield high-momentum associated hadrons. The current understanding of jet-medium interactions indicates that in-medium energy loss by high-energy partons is the cause of the suppression in the yield of high-momentum hadrons. However, as shown in [2], models can reproduce the enhancement measured at low momentum by including a mechanism by which energy embedded into the medium by hard partons is redistributed into the production of soft particles as a medium response. Unlike in Ref. [2], in which the $I_{AA}(p_{T,h})$ is measured as a function of $\xi = -ln(z_T)$, where z_T is the fraction of p_T carried by the final hadron relative to the hard-scattered parton, the transition from enhancement to suppression is shown in Fig. 4 to occur at a consistent $p_{T,h}$ of 1–2 GeV/c in each π^0 momentum range. This indicates a constant medium response that is independent of the jet energy.

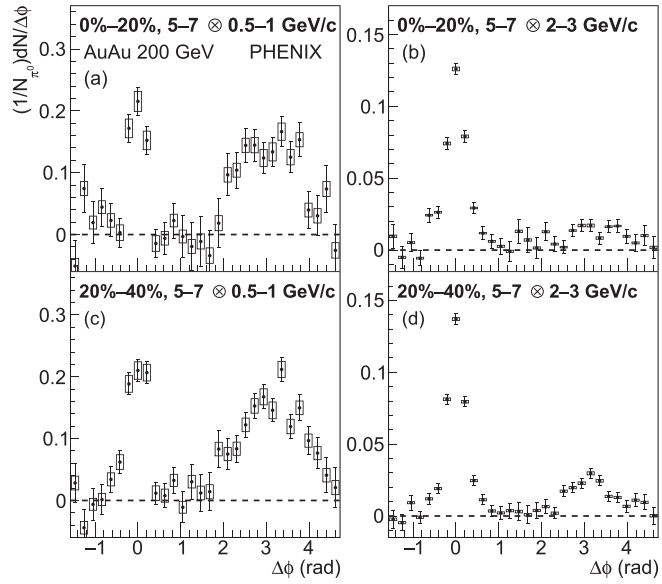

FIG. 3. Per-trigger jet-pair yield as a function of $\Delta\phi$ for selected π^0 trigger and charged-hadron-associated p_T combinations ($p_{T,\pi^0} \otimes p_{T,h}$) in Au + Au collisions. Statistical and systematic uncertainties are drawn as vertical lines and boxes, respectively. A global scaling uncertainty of 6.9% is not shown.

Lastly, the integrated away-side I_{AA} is measured in the 0%–20% and 20%–40% centrality bins, which are shown in Fig. 4 as circle (black) and diamond (red) points, respectively. There is no significant centrality dependence observed but for $p_{T,h} > 2$ GeV/c, the $I_{AA}(p_{T,h})$ in the 20%–40% bin is systematically closer to unity than in the 0%–20% bin. This difference in suppression levels could be attributed to a greater overall path length traversed by hard-scattered partons in the more central collisions, which in turn leads to greater energy loss, and a lower $I_{AA}(p_{T,h})$ value. This result is qualitatively in agreement with results from both the STAR [3] and ALICE [19] collaborations. The difference in the magnitude of the enhancement measured by the ALICE experiment (a factor of ≈5) vs here (a factor of ≈2) could arise due to differences in the plasmas created at the LHC and RHIC, such as the mean path length traversed by hard partons being larger, leading to an increased production of low-p_T hadrons. Similarly, the large enhancement measured in this result versus

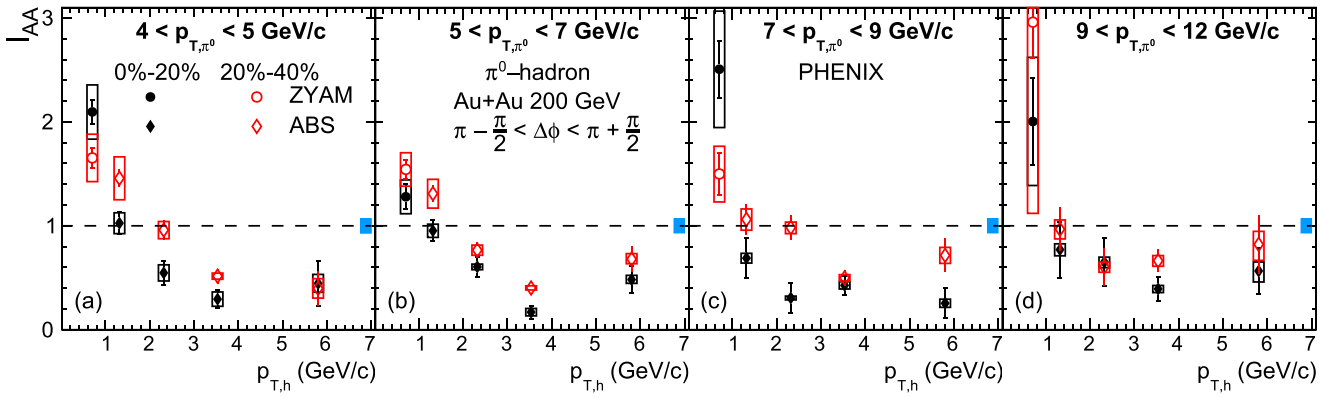

FIG. 4. Integrated away-side I_{AA} as a function of $p_{T,h}$. The π^0 trigger p_{T,π^0} range is shown at the top of each panel. Statistical and systematic uncertainties are drawn as vertical lines and boxes, respectively. A global scaling uncertainty of 6.9% is drawn as a blue box on the right of each panel at $I_{AA} = 1$.

that seen by the STAR experiment in Ref. [3] is due to the fact that this measurement extends down to a hadron momentum of 0.5 GeV/c, where the enhancement is very strong; whereas the threshold is at 1.2 GeV/c in the STAR result, where the I_{AA} is closer to unity.

Figure 5 shows the I_{AA} as a function of $\Delta\phi$, $I_{AA}(\Delta\phi)$, for three $p_{T,h}$ ranges, four p_{T,π^0} ranges, and two centrality classes. This observable allows for quantification of the modification to the jet yield at different distances from the away-side jet axis ($\Delta\phi \approx \pi$). The $I_{AA}(\Delta\phi)$ shows an enhancement in the yield of low-momentum hadrons across the away-side jet peak, although this enhancement is strongest at wide angles relative to the peak. The away-side peak is also the first region where the $I_{AA}(\Delta\phi)$ begins to fall beneath unity as shown by the $1.0 \leqslant p_{T,h} < 2.0$ GeV/c (red diamonds) in both the 0%–20% and 20%–40% centrality bins. In the highest momentum bin reported, $3.0 \leqslant p_{T,h} < 5.0$ GeV/c, the yield of charged hadrons is suppressed across all angles shown, a result of the partonic energy loss induced by parton-medium interactions. In contrast, the enhancement is most severe at wide angles relative to the away-side jet peak similar to what is seen in Ref. [2].

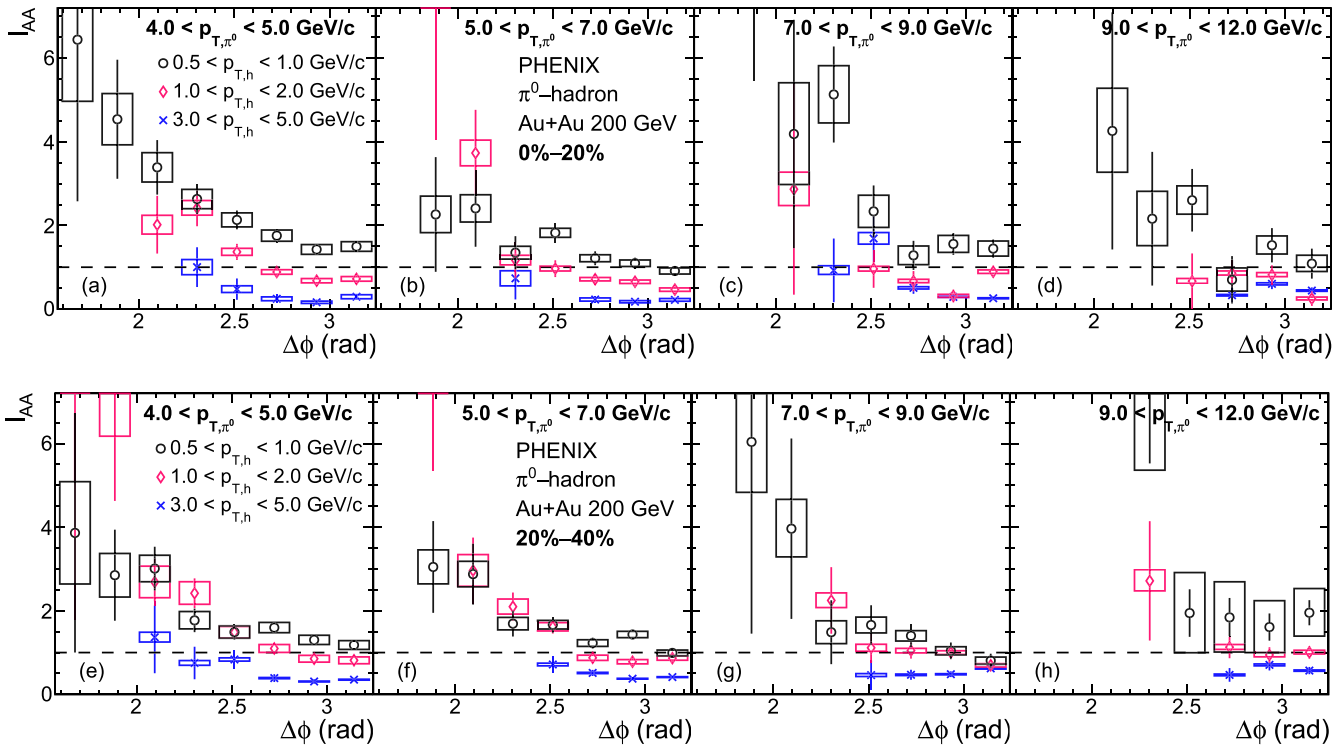

FIG. 5. Differential away-side I_{AA} as a function of $\Delta\phi$ in (a) to (d) 0%–20% and (e) to (h) 20%–40% centrality classes. The π^0 trigger p_{T,π^0} range is shown at the top of each panel. Statistical and systematic uncertainties are drawn as vertical lines and boxes, respectively. A global uncertainty of 6.9% is not shown.

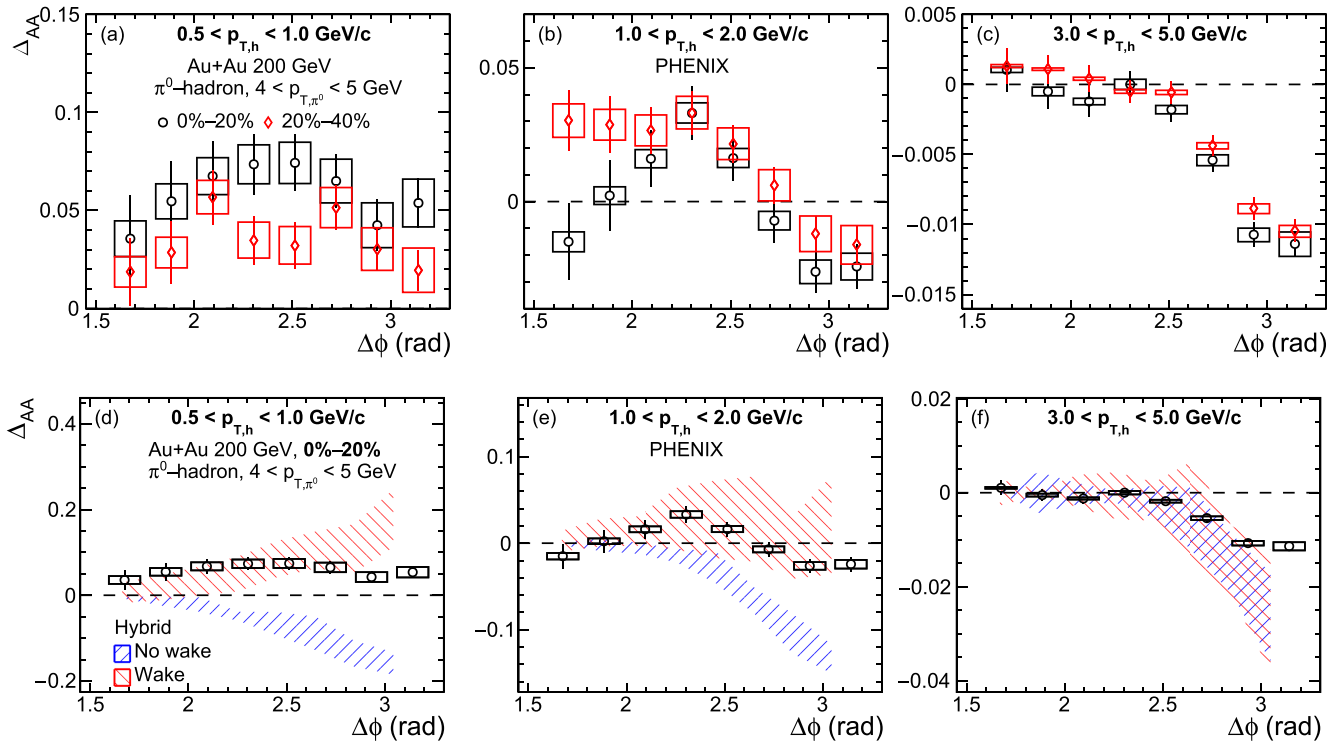

FIG. 6. (a)–(c) Differential away-side Δ_{AA} in 0%–20% (circles [black]) and 20%–40% (diamonds [red]) centrality classes for $\pi/2 < \Delta\phi < \pi$. (d)–(f) Differential away-side Δ_{AA} in 0%–20% centrality class for the same $\Delta\phi$ range compared to hybrid models with "Wake" (backward [red] slashes) and "No wake" (forward [blue] slashes). A global uncertainty of 6.9% is not shown.

Figure 6 shows the difference between Au + Au and $p + p$ in the per-trigger yield, Δ_{AA}, as a function of $\Delta\phi$ for hadrons with $0.5 < p_T < 1$ GeV/c. The enhancement (where the difference between the Au + Au and $p + p$ yields is positive) is again observed over a wide range of angles. The enhancement increases when moving away from the away-side jet axis, that is $\Delta\phi = \pi$. The enhancement seen at wider angles is also consistent with the phenomena of jet broadening. It is notable that the enhancement is observed near the $\Delta\phi = \pi/2$ region because, as shown in Fig. 3, that is the minimum of the per-trigger jet-pair yield. One key advantage of taking the difference in Au + Au and $p + p$ over computing the I_{AA} is that it is less sensitive than the I_{AA} to the $p + p$ yields fluctuating close to zero, particularly near $\Delta\phi = \pi/2$. This approach provides stronger constraints on theoretical models than the I_{AA} in these regions. The modification seen in Fig. 6 is further explored by observing how the measurement changes as a function of hadron p_T.

Figure 6 shows the difference in the per-trigger yields between Au + Au and $p + p$ as a function of $\Delta\phi$ for different $p_{T,h}$ bins associated with 4–5 GeV/c π^0, which clearly demonstrates the transition from enhancement at low $p_{T,h}$ to suppression at high $p_{T,h}$. In particular, the suppression in the per-trigger yield is most severe near the jet axis ($\Delta\phi \approx \pi$). This suppression pattern differs slightly from that seen in measurements at the LHC, such as in [20], where the yield of hadrons within a jet is found to be almost unmodified at the jet axis, regardless of the momentum range. However, for these RHIC results the I_{AA} and Δ_{AA} vs $\Delta\phi$ are measured from the recoil jet opposite the jet containing the trigger π^0, which imposes almost no bias on the recoil jet. Note that anti-k_T jets like those measured in Ref. [20] have more stringent requirements and could bias the sample of reconstructed jets in Au + Au to be more similar to those in $p + p$ collisions.

Figure 6(d) to 6(f) show the Au + Au and $p + p$ yield differences versus $\Delta\phi$ for selected $p_{T,\pi^0} \otimes p_{T,h}$ bins overlaid with calculations from the HYBRID model [9] (all available $p_{T,\pi^0} \otimes p_{T,h}$ bins are shown in Figs. 7 and 8). This model uses a combination of perturbative quantum chromodynamics and anti–de Sitter/conformal field theory to handle hard and soft interactions within the medium, respectively. One can see that at high $p_{T,h}$, the HYBRID model reproduces the data well within the uncertainty of the model. Two versions of the model are presented, differentiated by how they handle the medium response to the embedded partonic energy by the hard-scattered parton. The curve labeled "Wake" models a medium response to the lost energy as a hydrodynamic wake of soft particles, which well reproduces the wide-angle enhancement seen in the data at low $p_{T,h}$. The curve labeled "No wake" does not include this effect, and, thus, fails to reproduce the data at low $p_{T,h}$. The success of this model at low $p_{T,h}$ relies on a qualitatively similar mechanism as the CoLBT-Hydro model shown in Ref. [2]. Both models include hydrodynamic responses from the medium that contribute to the creation of an excess of soft particles in the final-state particle distribution.

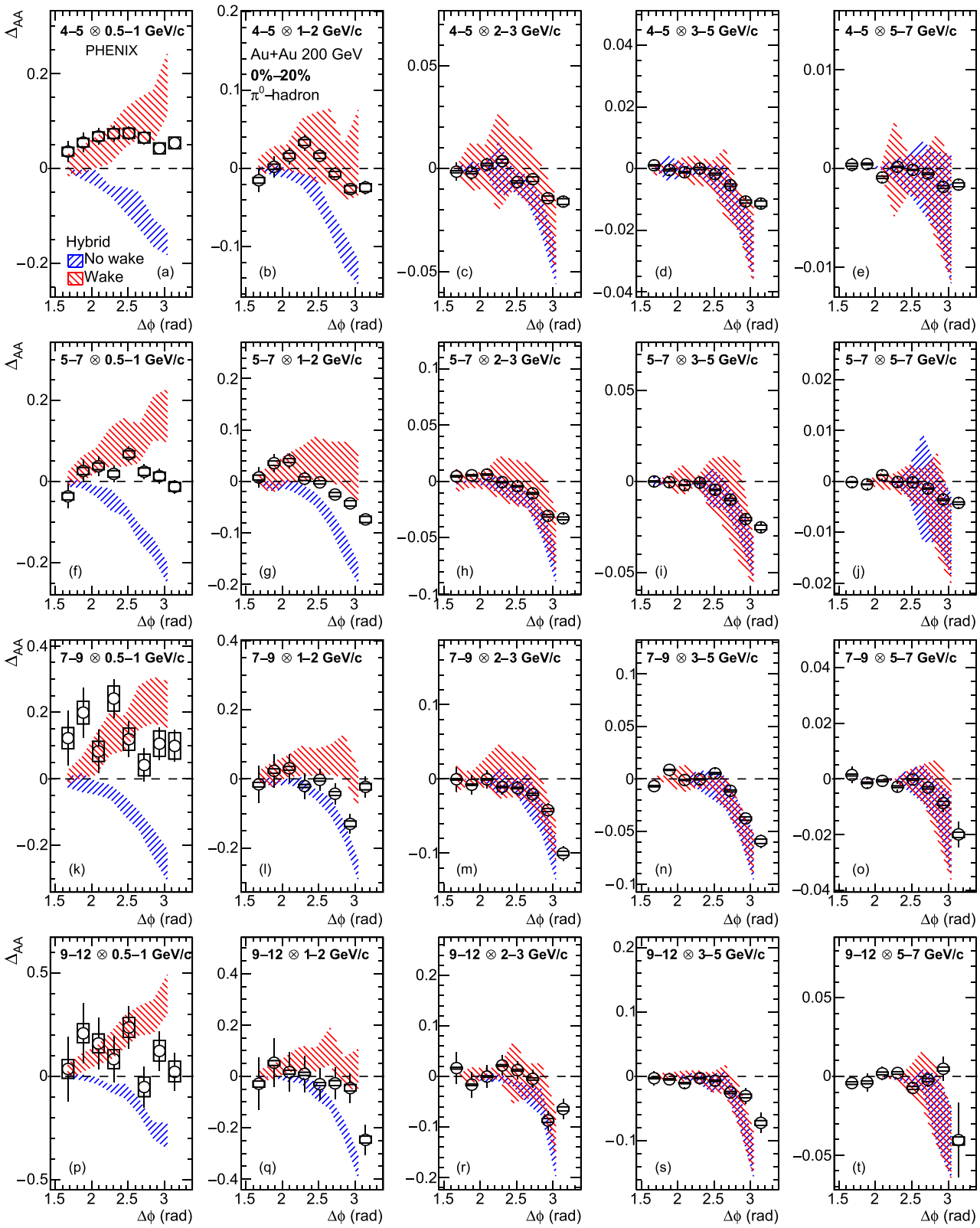

FIG. 7. Differential away-side Δ_{AA} in 0%–20% centrality for $\pi/2 < \Delta\phi < \pi$ for various π^0 trigger and charged-hadron-associated p_T combinations ($p_{T,\pi^0} \otimes p_{T,h}$). As in Fig. 6(d)–6(f), the "Wake" and "No wake" hybrid models are overlaid as backward (red) slashes and forward (blue) slashes.

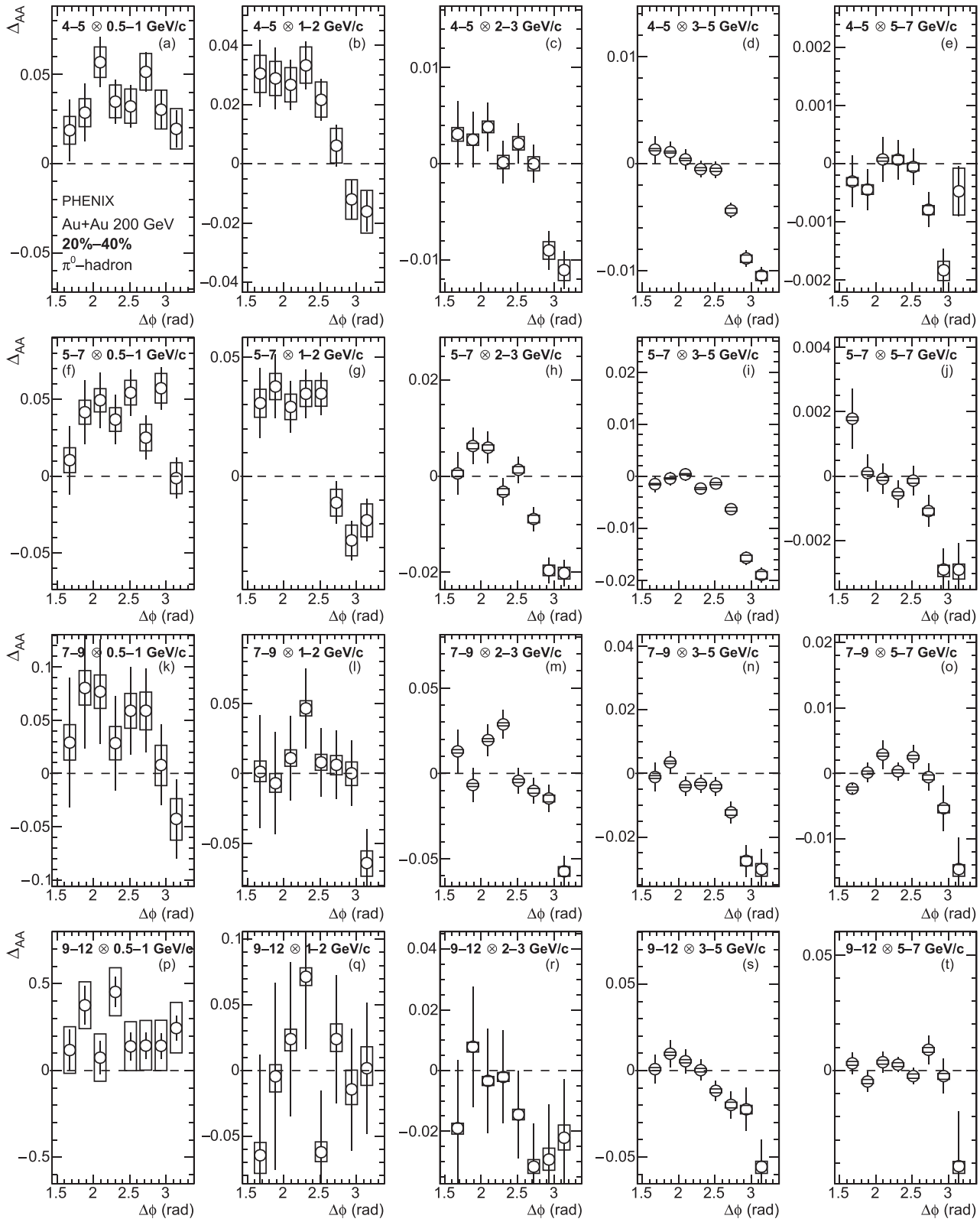

FIG. 8. Differential away-side Δ_{AA} as a function of $\Delta\phi$ in 20%–40% centrality for various π^0 trigger and charged-hadron-associated p_T combinations ($p_{T,\pi^0} \otimes p_{T,h}$).

VI. SUMMARY

The PHENIX collaboration presented a new π^0-hadron correlation measurement in Au + Au collisions at 200 GeV with data taken in 2014 at RHIC. With the enhanced statistics of the 2014 data set and improved background subtraction that accounts for contributions from flow up to the fourth-order flow coefficient, the results presented here are an improvement over previous PHENIX measurements. These jet functions and their integrated yields are then used to calculate both the quotient, I_{AA}, and the difference, Δ_{AA}, between Au + Au and $p + p$ yields vs $\Delta\phi$ (as well as the I_{AA}) as a function of the associated-hadron p_T.

The integrated per-trigger-yield modification, I_{AA} as a function of $p_{T,h}$, is indicative of partonic energy loss by hard partons via parton-medium interactions, leading to the suppression of hard jet particles and enhancement of soft jet particles. The new observables, differential per-trigger-yield modifications as a function of $\Delta\phi$, show the modifications are angularly dependent within the recoil jets. The angular dependence of I_{AA} and Δ_{AA}, also changes with jet-particle transverse momentum. The transition from enhancement of low-momentum particles to suppression at higher momentum is consistent with models such as the HYBRID model that include medium response. The differential I_{AA} is sensitive to the small modification at the edge of the jets, while the differential Δ_{AA} is less sensitive to statistical fluctuations. Using a variety of jet related observables will further constrain the models in the study of jet modifications, allowing for a more precise determination of QGP properties.

ACKNOWLEDGMENTS

We thank the staff of the Collider-Accelerator and Physics Departments at Brookhaven National Laboratory and the staff of the other PHENIX participating institutions for their vital contributions. We acknowledge support from the Office of Nuclear Physics in the Office of Science of the Department of Energy, the National Science Foundation, a sponsored research grant from Renaissance Technologies LLC, Abilene Christian University Research Council, Research Foundation of SUNY, and Dean of the College of Arts and Sciences, Vanderbilt University (USA), Ministry of Education, Culture, Sports, Science, and Technology and the Japan Society for the Promotion of Science (Japan), Conselho Nacional de Desenvolvimento Científico e Tecnológico and Fundação de Amparo à Pesquisa do Estado de São Paulo (Brazil), Natural Science Foundation of China (People's Republic of China), Croatian Science Foundation and Ministry of Science and Education (Croatia), Ministry of Education, Youth and Sports (Czech Republic), Centre National de la Recherche Scientifique, Commissariat à l'Énergie Atomique, and Institut National de Physique Nucléaire et de Physique des Particules (France), Bundesministerium für Bildung und Forschung, Deutscher Akademischer Austausch Dienst, and Alexander von Humboldt Stiftung (Germany), J. Bolyai Research Scholarship, EFOP, HUN-REN ATOMKI, NKFIH, and OTKA (Hungary), Department of Atomic Energy and Department of Science and Technology (India), Israel Science Foundation (Israel), Basic Science Research and SRC(CENuM) Programs through NRF funded by the Ministry of Education and the Ministry of Science and ICT (Korea). Physics Department, Lahore University of Management Sciences (Pakistan), Ministry of Education and Science, Russian Academy of Sciences, Federal Agency of Atomic Energy (Russia), VR and Wallenberg Foundation (Sweden), University of Zambia, the Government of the Republic of Zambia (Zambia), the U.S. Civilian Research and Development Foundation for the Independent States of the Former Soviet Union, the Hungarian American Enterprise Scholarship Fund, the US-Hungarian Fulbright Foundation, and the US-Israel Binational Science Foundation.

[1] M. Connors, C. Nattrass, R. Reed, and S. Salur, Jet measurements in heavy ion physics, Rev. Mod. Phys. **90**, 025005 (2018).
[2] U. Acharya *et al.* (PHENIX Collaboration), Measurement of jet-medium interactions via direct photon-hadron correlations in Au + Au and d + Au collisions at $\sqrt{s_{NN}} = 200$ GeV, Phys. Rev. C **102**, 054910 (2020).
[3] L. Adamczyk, Jr. *et al.* (STAR Collaboration), Jet-like correlations with direct-photon and neutral-pion triggers at $\sqrt{s_{NN}} = 200$ GeV, Phys. Lett. B **760**, 689 (2016).
[4] J. Adam *et al.* (ALICE Collaboration), Measurement of jet suppression in central Pb-Pb collisions at $\sqrt{s_{\rm NN}} = 2.76$ TeV, Phys. Lett. B **746**, 1 (2015).
[5] G. Aad *et al.* (ATLAS Collaboration), Observation of a centrality-dependent dijet asymmetry in lead-lead collisions at $\sqrt{s_{NN}} = 2.77$ TeV with the ATLAS Detector at the LHC, Phys. Rev. Lett. **105**, 252303 (2010).
[6] S. Chatrchyan *et al.* (CMS Collaboration), Observation and studies of jet quenching in PbPb collisions at nucleon-nucleon center-of-mass energy = 2.76 TeV, Phys. Rev. C **84**, 024906 (2011).
[7] K. M. Burke *et al.* (JET Collaboration), Extracting the jet transport coefficient from jet quenching in high-energy heavy-ion collisions, Phys. Rev. C **90**, 014909 (2014).
[8] W. Chen, Z. Yang, Y. He, W. Ke, L. G. Pang, and X.-N. Wang, Search for the elusive jet-induced diffusion wake in Z/γ-jets with 2D jet tomography in high-energy heavy-ion collisions, Phys. Rev. Lett. **127**, 082301 (2021).
[9] J. Casalderrey-Solana, D. C. Gulhan, J. G. Milhano, D. Pablos, and K. Rajagopal, A hybrid strong/weak coupling approach to jet quenching, J. High Energy Phys. 10 (2014) 019; 09 (2015) 175.
[10] A. Adare *et al.* (PHENIX Collaboration), Transition in yield and azimuthal shape modification in dihadron correlations in relativistic heavy ion collisions, Phys. Rev. Lett. **104**, 252301 (2010).
[11] M. Allen *et al.* (PHENIX Collaboration), PHENIX inner detectors, Nucl. Instrum. Methods Phys. Res. A **499**, 549 (2003).
[12] K. Adcox *et al.* (PHENIX Collaboration), PHENIX central arm tracking detectors, Nucl. Instrum. Methods Phys. Res. A **499**, 489 (2003).

[13] A. Sickles, M. P. McCumber, and A. Adare, Extraction of correlated jet pair signals in relativistic heavy ion collisions, Phys. Rev. C **81**, 014908 (2010).

[14] B. I. Abelev *et al.* (STAR Collaboration), System-size independence of directed flow measured at the BNL Relativistic Heavy-Ion Collider, Phys. Rev. Lett. **101**, 252301 (2008).

[15] L. Adamczyk *et al.* (STAR Collaboration), Beam-energy dependence of the directed flow of protons, antiprotons, and pions in Au+Au collisions, Phys. Rev. Lett. **112**, 162301 (2014).

[16] A. Adare *et al.* (PHENIX Collaboration), Measurement of two–particle correlations with respect to second- and third-order event planes in Au+Au collisions at $\sqrt{s_{NN}} = 200$ GeV, Phys. Rev. C **99**, 054903 (2019).

[17] A. Adare *et al.* (PHENIX Collaboration), Azimuthal anisotropy of π^0 production in Au + Au collisions at $\sqrt{s_{NN}} = 200$ GeV: Path-length dependence of jet quenching and the role of initial geometry, Phys. Rev. Lett. **105**, 142301 (2010).

[18] R. A. Lacey, A. Taranenko, J. Jia, N. N. Ajitanand, and J. M. Alexander, Scaling of the higher-order flow harmonics: implications for initial-eccentricity models and the "viscous horizon", arXiv:1105.3782v2.

[19] J. Adam *et al.* (ALICE Collaboration), Jet-like correlations with neutral pion triggers in *pp* and central Pb-Pb collisions at 2.76 TeV, Phys. Lett. B **763**, 238 (2016).

[20] G. Aad *et al.* (ATLAS Collaboration), Measurement of angular and momentum distributions of charged particles within and around jets in Pb + Pb and *pp* collisions at $\sqrt{s_{NN}} = 5.02$ TeV with the ATLAS detector, Phys. Rev. C **100**, 064901 (2019).